SolarPACES 2024, 30th International Conference on Concentrating Solar Power, Thermal, and Chemical Energy Systems

Thermal Energy Storage Materials, Media, and Systems

https://doi.org/10.52825/solarpaces.v3i.2389

© Authors. This work is licensed under a Creative Commons Attribution 4.0 International License

Published: 18 Nov. 2025

Hot Corrosion and Mechanical Performance of Aluminide Coated Austenitic Steel

Loïc Oger^{1,*} (10), Alina Agüero¹ (10), and Pauline Audigié¹ (10)

¹Instituto Nacional de Técnica Aeroespacial (INTA), Spain

*Correspondence: Loïc Oger, loge@inta.es

Abstract. The present study aims at improving coatings to allow higher operating temperatures – up to 700 °C – while resisting hot corrosion in future heat transfer fluids and storage systems for CSP technology. An aluminide coating was produced onto a 347H austenitic alloy to resist Li-Na-K molten carbonate corrosion at 700 °C. Multiple surface preparations were investigated and, after optimization, a new diffusion heat treatment was selected. A homogeneous 3-layer coating was formed with Al content reaching up to 69 at.% at the top surface. Corrosion was significantly decreased by the coating compared to the uncoated material. After 500h-exposure, a 100 μm-thick multi-layered and non-adhesive alkali elements rich oxide formed at the surface of uncoated 347H alloy. On the contrary, the coated material preserved its morphology and a mix of α-LiAlO₂ and γ-LiAlO₂ formed on the top coating. From the mechanical perspective, local hardness measurements highlighted a broad variation along the different layers of the coating. 3-point bending tests showed that deformation in the plastic domain was required to cause crack formation. Cracks remained in the two outermost layers of the coating and did not reach the underneath substrate.

Keywords: Carbonate Molten Salt, Slurry Aluminide Coating, Austenitic Steel

1. Introduction

With the need for the European energy system to become more climate resilient and diversify energy sources, Concentrated Solar Power (CSP) has attracted growing interest [1], [2]. Since the 1980s, CSP technology combined with thermal energy storage (TES) systems has considerably evolved, becoming more reliable, efficient and able to store energy for longer durations [3]. However, its share in the renewable energy market remains too low and the need for expensive materials capable of withstanding operating conditions makes it uncompetitive and limits a wider range use [4]. Indeed, corrosive molten salts are used as heat transfer fluids (HTF) and storage media to transport energy to a power turbine to produce electricity. The European post-doctoral fellowship COMETES aims to address both issues by developing low-cost coated materials suitable in current and harsher operating conditions, considered for next-generation plants.

Slurry aluminide coatings have been shown to significantly improve the hot corrosion resistance of ferritic steels exposed to Solar Salt (60 wt% NaNO₃ – 40 wt% KNO₃) up to 580 °C [5]. However, reaching higher efficiencies would require the use of thermodynamic cycles operating at temperatures over 700 °C [6]. Under these conditions, nitrate mixtures are unstable, decomposing into nitrites (NO₂-), which increase corrosiveness and degrade their thermophysical properties. Among other candidates, Li-Na-K carbonate mixtures have emerged as one of the most promising solution for future HTF and TES media [7], [8]. Their viscosity is compatible

with pumping systems and their high heat capacity reduces the molten salt amount required for a similar storage duration. However, the resulting new operating conditions also raise the corrosion rates, thus an optimization in CSP components design is required [9]. Indeed, ferritic alloys are unsuitable due to their low corrosion resistance in those conditions but also due to their low creep resistance over 600 °C [10]. Some authors worked on decreasing the salt corrosivity to reduce its impact on the material degradation [11] or using surface modified Nibased alloys to resist such conditions [12], but those solutions still remain expensive.

Studies have shown that austenitic steels offer satisfactory hot corrosion resistance in currently used Solar Salt at 565°C [13] explaining why such alloys, like 347H especially, are used for components in direct contact with molten salts in hot storage tanks. However, in Li-Na-K carbonate mixtures, austenitic steels underwent rapid deterioration and form multilayered alkali element rich corrosion scales [14], [15]. Material loss between 150 and 466 µm/year – depending on the exposure conditions – were measured. During the corrosion process, outward Cr-diffusion was observed, leading, for long-term exposure, to significant Cr VI contamination of the salt. This needs to be limited for safety reasons (REACH regulation) and expensive processes are required for salt decontamination once its service life is over. Finally, contaminants such as Mg were also detected as dissolved into the melt, limiting the lifetime of the CSP components by increasing corrosion rates [16].

The objective of this study is to improve austenitic steel hot carbonate corrosion resistance by using slurry aluminide coatings. Coated solutions have been widely used on ferritic steels and have demonstrated their efficiency to resist hot corrosion in Solar Salt [5], [17], [18]. However, few works have focused on austenitic steels at higher operating temperatures and coating process optimization remains an issue for further industrial applications. Thereby, the present work focuses on optimizing the coating deposition process on a 347H alloy. The coating suitability was evaluated on the basis of microstructural observations, 500h-hot corrosion tests in carbonates (32.1wt% Li₂CO₃, 33.4wt% Na₂CO₃, 34.5 wt% K₂CO₃) at 700 °C in static conditions and mechanical tests performed before and after hot corrosion exposure.

2. Materials and experimental method

2.1 Substrate

The composition of 347H steel is given in Table 1. It is a Nb- stabilized austenitic steel. A minimal stoichiometric ratio Nb/C (min 7.7 in weight) is maintained to favour Nb-rich carbide precipitation and make carbon unavailable for more detrimental carbides. Lower Nb contents could increase the susceptibility to intergranular corrosion of the steel, whereas high Nb-contents could favour the formation of Laves phases (Fe_2Nb) known to be detrimental for the steel mechanical resistance and especially hot cracking [19]. Ni (10 wt.%) is added to enhance cracking resistance, Cr improves its corrosion and high-temperature oxidation resistance, and Mo addition allows a higher resistance to pitting corrosion.

Table 1. Chemical composition (wt.%) of 347H measured by XRF.

Fe	Ni	Cr	С	Mn	Мо	Si	Р	S	Nb	Al	Cu
Base	9.5	17.3	0.05	1.40	0.31	0.32	0.03	0.0005	0.54	0.03	0.30

347H steel coupons (20x10x3 mm) were cut from 3 mm-thick plates and then ground with SiC paper grade 180. Before coating and exposure in molten salts, the samples were cleaned for 5 min in an ethanol ultrasonic bath and dried in air.

2.2 Coating deposition

Before coating, various surface preparation methods were evaluated on 347H austenitic steel to optimize the coating microstructure and to comply with industrial practices and requirements as well as laboratory research:

- Grinding with P180 SiC paper (reference surface preparation)
- Grit blasting:
 - o with Al₂O₃ particles followed by glass beading.
 - o with SiC particles
 - o with angular martensitic steel grit
- Chemical attack consisting in 15 min exposure in NaOH 1M at 70-80 °C followed by 10 min exposure in HCl 10 wt.% at room temperature.

Roughness was measured after surface preparation with a Time 3200/3202 surface roughness tester prior to coating deposition. The aluminide coating was applied by spraying a proprietary Cr VI-free, water-based Al slurry developed at INTA. The slurry was prepared by mixing Al powder (Ø: 5 μ m, 99 wt% obtained from Poudres Hermillon) with water and an inorganic binder. An average slurry thickness of 150 μ m was sprayed onto each side of the samples. The coated samples were then dried under laboratory air for 1 h. A two-step diffusion heat treatment was subsequently carried out under Ar at 700 °C for 2 h and 950 °C for 15 min.

2.3. Molten salt corrosion testing

The hot corrosion resistance of coated and uncoated 347H steel was investigated by immersing the samples in a ternary carbonate eutectic mixture (32.1wt% Li_2CO_3 – 33.4wt% Na_2CO_3 – 34.5wt% K_2CO_3) at 700 °C under static conditions up to 500 h. Two types of experiments were performed for both types of specimens: 1) isothermal exposure up to 500 h and 2) interrupted tests at 24, 48, 96, 168, 241 and 500 h during which the coupons were removed from the salt, cleaned, weighted and then re-immersed to estimate the degradation kinetic. For each condition, two identical specimens were fully immersed in a 30 mL alumina crucible filled with salt and then placed in a Carbolite muffle furnace with a continuous monitoring of the test temperature. The level of molten salt in each crucible was controlled every two weeks as salts slightly evaporated, and the crucibles were refilled each time it was considered necessary to maintain the same salt level in the crucibles all along the tests. Before weighting, salt residues on the surface were removed by cleaning the specimen in hot distilled water at 80 °C.

2.4. Mechanical characterization

Vickers microhardness was measured with a 50 g-load to monitor the evolution of the local mechanical properties along the developed coating. These tests were performed according to UNE-EN ISO 6507-1 standard [20] with a MTS test device. A minimum of 40 measurements was obtained in the substrate and in each layer of the coating. Additional local Vickers hardness measurements with a 10 g-load were performed in the top layer of the produced coating to distinguish the different phases composing it. Considering the small area of each phase, only 1 or 2 measurements were made with 10 g-load leading to no consistent standard deviation. These tests were only used as discussion elements.

Three-point bending tests were also carried out on coated specimens at different strain levels, 1.3, 2.2 and 4.5%, which, according to Fig.1, correspond to the elastic, elasto-plastic and plastic domains of the substrate, respectively. These tests were performed to investigate the possible crack formation in the coating. Specific parallelepiped samples (100x10x6 mm) were designed for bending. Their surface was prepared by grinding with P180 SiC paper and

the coating was applied on one side of the samples by spraying. The bending tests were conducted so that the coated side was subjected to tensile stresses, intentionally inducing crack formation.

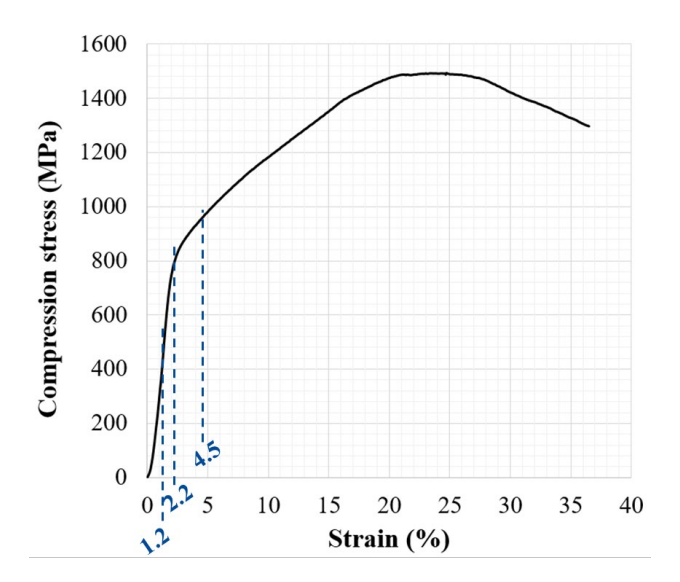


Figure 1. Stress-strain curves obtained by 3-point bending of uncoated 347H.

2.5. Microstructural characterization

Optical and digital microscopes (Leica MEF4M and Leica DVM6) were used to characterize the cracks formed after the bending test. Field emission scanning electron microscopy (FESEM, Thermofischer Scientific Apreo C LoVac) associated to energy-dispersive X-ray spectroscopy (EDS, Oxford Instruments Aztec) was used to characterize the samples microstructure, the developed coatings and the corrosion scales formed after hot corrosion tests. This was coupled with surface X-ray diffraction (XRD) analysis to characterize the coating's phases and the corrosion scales. The latter was performed at room temperature with a θ - θ mounting, from 20° to 120° with a 0.5° step and a 2 second holding time, using a Panalytical X'Pert, Cu K α ₁ (1.5406 Å).

Fig.2 summarizes the experimental procedure implemented in the present study.

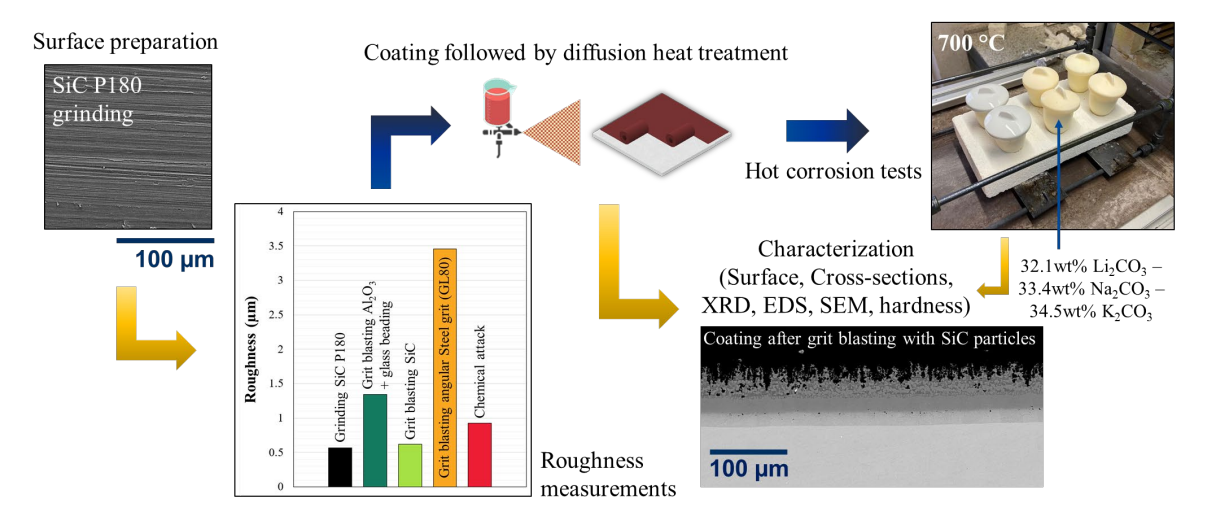


Figure 2. Schematic representation of the experimental procedure, including roughness measurements and SEM micrographs of a 347H ground surface (SiC P180) and of a cross section of a coating produced on a surface grit blasted with SiC particles.

3. Results and discussion

3.1 Coating development

Roughness measurements were carried out after surface preparation to get a preliminary ranking, as previous works showed an improved coating application for roughness < 1 μ m on ferritic steels [21]. Fig.2 shows that grit blasting led to roughness between 1.3 and 3.5 μ m except when using SiC particles which resulted in a significantly lower roughness of 0.7 μ m (surface presented in Fig.2). However, all the coatings applied on the grit blasted surfaces had a lack of uniformity and did not adhere well. In particular, in the case of alumina grit blasting, it was observed that remaining Al₂O₃ particles at the alloy surface blocked the slurry diffusion during the heat treatment subsequent to spraying, which is consistent with previous results [21]. Glass beading after blasting, allowed to decrease this effect and to improve the surface roughness, but difficulties were found to remove all embedded alumina particles from the surface with this method. On the contrary, the coatings obtained on ground and chemically attacked surfaces offered good results, the latter being considered for future industrial application.

Fig.3 shows the coating obtained on the P180 SiC ground surface after diffusion heat treatment and elimination of slurry residues. A 3-layer aluminide coating formed with various concentrations of Al, Fe, Cr and Ni, with an approximate thickness of 100 μ m (Fig.3a). No cracks were observed in the coating.

The top layer (Fig.3c) is composed by 3 phases with high Al amounts varying between 50 and 69 at% from the lightest to the darkest phase (Table 2). XRD measurements (Fig.3e) revealed the presence of Fe_2Al_5 (Fig.3a, spot 1), as well as Fe- and Al-rich intermetallic phases FeAl, $FeAl_{2.7}$, which stoichiometry was not clearly identified neither accurately linked with the contrasts observed on backscattered electron image provided in Fig.3a (spots 2 and 3). Indeed, both $FeAl_2$ and $FeAl_3$ seem to fit with the XRD pattern obtained. EDS spot measurements (Fig.3d) suggest that the darkest phase is Fe_2Al_5 and the lightest is FeAl. The intermediategrey phase was observed to be Cr-rich (Table 2) with a stoichiometry close to Al_2FeCr , although not confirmed by XRD. This Cr-rich phase requires further investigation.

The intermediate layer (\sim 30 µm) has a composition (Fe-Al, 50-35 at.%, Table 2) very close to the light phase composing the top layer, suggesting that both are identical. In analogy to other works [17], it was identified as *FeAl* (spot 4). Finally, the inner layer (\sim 25 µm) which contains up to 15 at.% of Al (Fig. 3a, spot 5) is also rich in *FeAl* precipitates with the same composition as the intermediate layer, based on SEM images and EDS analyses.

Table 2. Chemical composition (at. %) of the main three phases composing the aluminide coating, according to EDS measurements.

Phase	Spot	Al	Fe	Cr	Ni
Top layer – Dark grey	1	69	27	3	0.5
Top layer – Intermediate-	2	55	25	17	1
grey					
Top layer – Light grey	3	50	33.5	7.5	7.5
Intermediate layer	4	50	35	7.5	5.5
Inner layer	5	14	59	20.5	4
Matrix	6	-	69	19	9

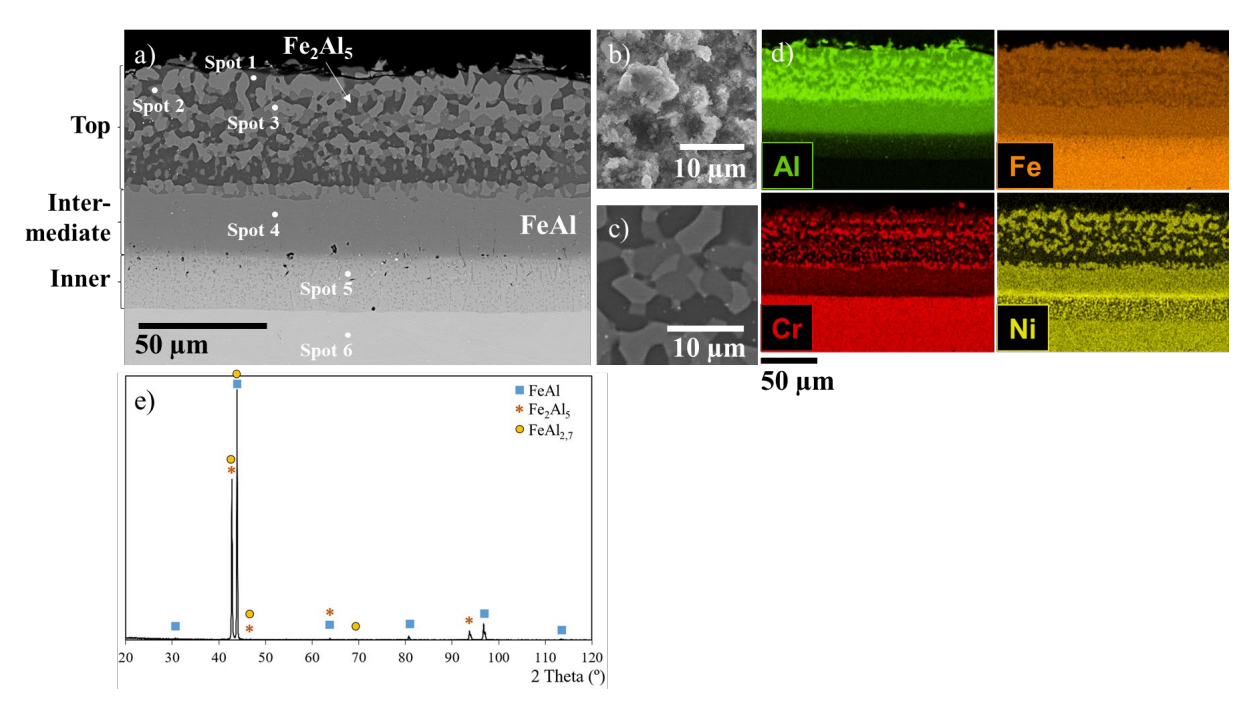


Figure 3. FESEM micrographs of cross-section of the aluminide coated 347H (SiC P180) after diffusion heat treatment of 2 h at 700 °C followed by 15 min at 950 °C in Ar: a) global coating, b) surface observation and c) zoomed-in view of the top layer, respectively. Figure d) is the EDS elemental mapping of Al, Fe, Ni and Cr from all the area shown in figure a). Figure e) is the corresponding surface XRD pattern.

3.2 Mechanical resistance

Given the fact that the coating is composed of 3 layers, some of which are multi-phased, the question of the mechanical resistance arises. In a first approach, measurements in each layer highlighted a very high hardness range in the as-coated samples, from 923 HV_{0.05} in the top layer to 407 HV_{0.05} in the inner layer (Fig.4). In addition, local hardness measurements with a 10 g-load were performed in the top layer to distinctly distinguish the mechanical properties of the constituent phases. Values of 1034 HV_{0.001} and 690 HV_{0.001} were obtained for the darkest (Fig.3a, spot 1) and lightest phases (Fig.3a, spot 3), respectively. In their paper, Matysik *et al.* [22] gathered the results of various studies related to the mechanical properties of Fe-Al intermetallic phases and they found out values of 900-1100 HV, for Fe₂Al₅, 691-980 for FeAl₃, and 400-530 for FeAl. This tends to confirm that the dark phase is Fe₂Al₅, and the lighter phase could be attributed to FeAl₃. Nevertheless, the phases recognized as FeAl and FeAl₃ are very close to be unequivocally identified. Further investigations by nano-indentation are currently underway to confirm the phase identification. It is therefore important to note that there is a dispersion of microhardness which could affect the deformation behavior possibly favouring crack initiation.

Three-point bending tests were carried on the coated samples to evaluate the brittleness of the coating and to characterize crack formation. First, a minimum strain level of 4.5% was required to form cracks which corresponds to the plasticity domain of the 347H substrate. Except for the welded zones [23], such mechanical stresses should not be reached in CSP operating conditions so that the mechanical resistance of the developed coating is compatible with the CSP application. However, crack formation and coating mechanical degradation needs to be investigated considering that damages can occur, particularly during the installation of the plant components (pipes etc.).

Fig.4 shows a FESEM micrograph of the coated 347H steel after 4.5 % of deformation. Cracks perpendicular to the tensile stress direction were observed in the two outermost layers

and stop at the interface between the intermediate and the inner layer or inside the latter. This raises the question of crack propagation due to the coating brittleness. Indeed, it could have a detrimental effect from the mechanical point of view, favouring crack initiation and then propagation into the substrate, leading to premature failure. An in-depth investigation of the macroscopic mechanical properties of aluminide coated 347H is therefore essential. In addition, secondary cracks parallel to the tensile stress direction were observed in the top layer. These cracks seem to follow specific propagation paths across the multiphased top layer. As said previously, Matysik *et al.* [22] measured the mechanical properties of various Fe-Al phases including $FeAl_2$ and Fe_2Al_5 . Based on length measurements of cracks formed at the corner of microhardness prints, they were able to calculate stress intensity factors, K_{IC} , finding values of 3.88 and 5.17 MPa.m^{-1/2} for $FeAl_2$ and Fe_2Al_5 , respectively. $FeAl_2$ might thus be more susceptible to crack initiation leading to preferential secondary cracks propagation in the top layer. Comparatively, the intermediate layer composed by a unique FeAl phase showed almost no secondary cracks. Additional investigation is ongoing to evaluate the combined hot corrosion and mechanical resistance of the degraded coating in carbonate molten salts at 700 °C.

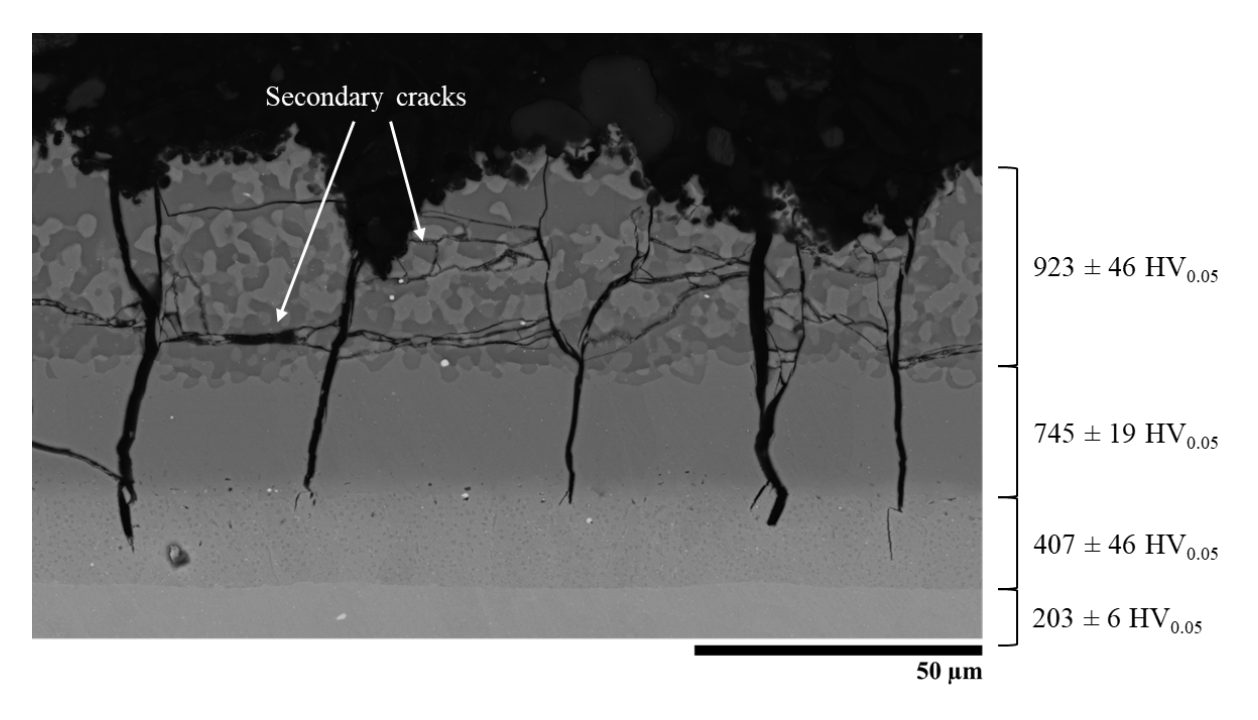


Figure 4. FESEM micrograph of a cross-section of the aluminide coated 347H after 3-point bending test at 4.5% of deformation. Average Vickers hardness values carried out with a 50 g-load in the ascoated sample are given for each layer.

3.3 Hot corrosion resistance

3.3.1 Gravimetric results after molten carbonate exposure

Gravimetric results of the isothermal and cyclic exposures of the coated and uncoated 347H in the Li-Na-K molten carbonate mixture at 700 °C are shown in Fig.5. The uncoated samples show a significant positive mass change (up to ~30 mg/cm²) which was attributed to the growth of a thick oxide scale at the alloy surface. On the contrary, the coated 347H steel performed well with a maximum positive mass gain measured of 0.6 mg/cm² after 500 h. This small mass increase remained quite constant along the cyclic exposure, and it is likely caused by remaining salt residues at the specimens' surface. Indeed, it was observed that carbonate salts, as soon as they froze, formed a hard and very adherent salt layer on the sample surface, somewhat difficult to remove from the exposed specimen, even in hot water.

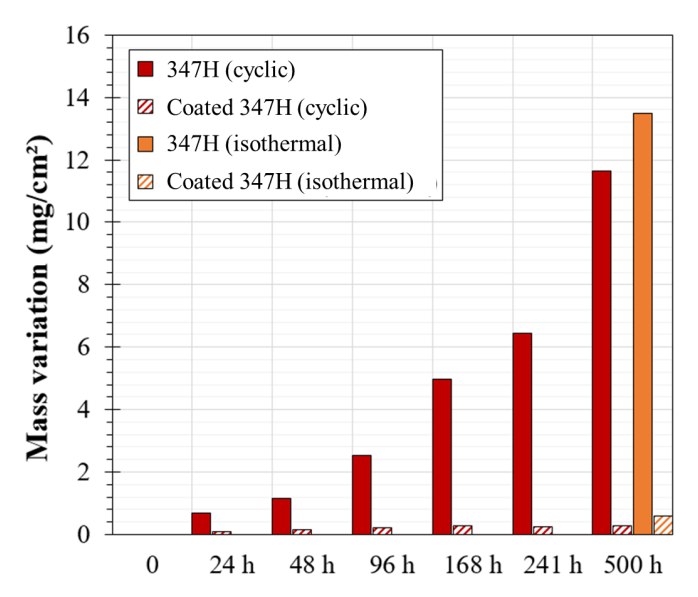


Figure 5. Mass variation of the coated and uncoated 347H during the isothermal and cyclic exposure at 700 °C in Li-Na-K molten carbonate salts.

3.3.2 Microstructures after exposure to molten carbonate salts

Fig.6 shows the microstructure and the EDS elemental maps of uncoated 347H steel after 500 h at 700 °C in molten carbonate salts. A very thick (\sim 100 µm) multi-layered oxide formed (Fig.6a) with a 2-layer outer oxide and a complex multi-phased inner oxide.

A thin Mn-rich oxide was highlighted on the top surface thanks to EDS mapping (Fig.6c). This demonstrates fast outward Mn-diffusion from the substrate and through the underlying oxide layer. Although it was not possible to clearly identify this Mn-rich layer by XRD at this stage, 1000-hours hot corrosion exposures allowed to identify $LiMnO_2$ as the main probable corrosion product formed.

Underneath, a thick Fe-rich, likely outer growing oxide formed due to outward Fe diffusion from the substrate to the surface and through the oxide scale. XRD analyses allowed identifying this layer as $LiFeO_2$ cubic phase (Fig.6d). For temperatures exceeding 600 °C, White *et al.* [24] reported that carbonate salts decompose according to reaction (2). The activity of the Li₂O in the eutectic mixture is known to be significantly higher than the activity of Na_2O and K_2O . At 700 °C, Li_2O dissociates into O^{2-} and Li^+ and the latter reacts with the surface oxide of the 347H alloy that formed according to reaction (1) at the melt/metal surface interface. This leads to the formation of Li-rich alkali oxides (reaction (3)), mainly.

$$2Mn^{+} + nO^{2-} \leftrightarrow 2MO_{n} \tag{1}$$

$$A_2CO_3 \leftrightarrow A_2O + CO_2$$
, with A= Li, Na or K (2)

$$Fe_2O_3 + O^{2-} + 2Li^+ \leftrightarrow 2LiFeO_2 \tag{3}$$

Although not clearly determined, other stoichiometry of Li-Fe-O oxides could form and fit with some remaining peaks of the XRD patterns –particularly $LiFe_5O_8$. Indeed, Luo *et al.* [14] observed that at 700 °C, the higher reactivity of O²⁻ and outward diffusion rate of Fe favoured the following reaction (4).

$$LiFeO_2 + 6O^{2-} + 4Fe^{3+} \leftrightarrow LiFe_5O_8$$
 (4)

As inner growing layer, an internal multi-phased oxide mainly rich in Cr and Fe formed which was analyzed by EDX measurements and compared with the literature. A Cr-rich layer was observed, possibly at the initial steel surface between the inner and the outer layers

(Fig.6c). This could be *LiCrO*₂, although the exposure duration is relatively short to observe this phase according to Sue *et al.* [25], or Biedenkopf *et al.* [26], and its solubility in molten carbonates is very high. This will be confirmed in a further study where gradual chemical oxide dissolution and XRD analysis will be conducted to identify all the corrosion products. Underneath, Fe- and Cr-depleted and Ni-rich unoxidized "islands" are visible in the inner oxide. As suggested by Luo *et al.* [14], intensive outward Fe-diffusion takes place to form *LiFeO*₂, while simultaneously inward O-diffusion occurs.

Finally, Cr-rich carbides were also observed at the grain boundaries (Fig.6b) of the steel below the oxide scale, which was expected as a typical evolution of the 347H steel microstructure after ageing at 700 °C. Those carbides probably correspond to $Cr_{23}C_6$ precipitates [27].

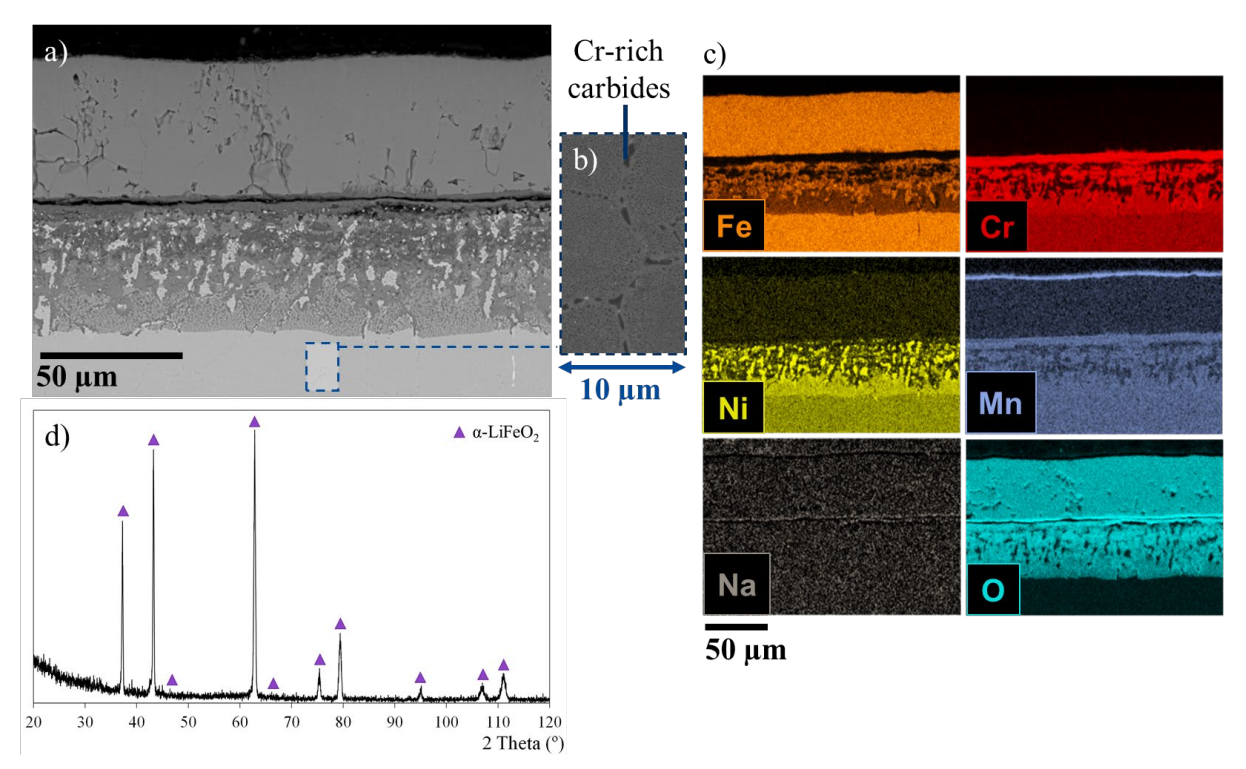


Figure 6. Analyses obtained on the uncoated 347H after 500 h in ternary carbonate mixture at 700 °C: a) and b) FESEM micrographs of oxide's cross-section and focus on intergranular Cr-carbides, respectively, c) is an EDS elemental mapping of Fe, Cr, Ni, Mn, Na and O from area in a), and d) is the corresponding surface XRD pattern.

Fig.7 shows the evolution of the coated material microstructure and composition after 500 h at 700 °C in molten carbonate salts. First, it is interesting to note that the slurry aluminide coating performed very well and its morphology remains similar to the as-coated state (Fig.3). Indeed, it appears that its thickness is stable, the coating is still composed of the three layers previously described with slight changes in Al contents. Only small changes are to be noticed after exposure.

Top surface observations of the coating (Fig.7b) evidenced the formation of cuboid-shaped oxides and very fine grains with a cauliflower morphology. In contrast, no oxide was observed on the as-coated surface (Fig.3b). XRD analyses (Fig.7e) associated to results obtained by others allowed to identify the cuboid features as γ -LiAlO₂ while the small grains were identified as α -LiAlO₂ which is known to be very stable at this temperature [28][29]. This is thus promising for longer-term exposure.

In addition, at 700 °C coating-substrate interdiffusion continued. Phase transformations have occurred in the outermost layer after 500 h, as the lighter, Al poorer phase has increased at the expense of Fe₂Al₅. The latter was confirmed by the XRD patterns, as the main Fe_2Al_5

peak at 43° appears to loose intensity after carbonate exposure (Fig.7e) compared to the ascoated sample (Fig.3e). Additionally, Cr and Si have segregated at the grain boundaries of the intermediate FeAl layer (Fig.7c), forming Cr₃Si precipitates (confirmed by XRD, Fig.7e). These precipitates were also observed in the outer layer at the interface between the darkest and the lightest phases (Fig.7c). A direct consequence of the diffusion process occurring during the molten salt exposure is the formation of voids, especially located near the interface between the intermediate and the inner layer but also within the top layer (Fig.7a). This can be interpreted as a Kirkendall effect likely associated to Al, Cr and Si diffusion. Similarly, the inner layer thickness increased in the substrate side. Given the limited changes observed and the formation of a protective oxide layer during exposure to carbonates, the developed coating shows promise as an alternative material. However, further investigation is needed, particularly with prolonged exposure.

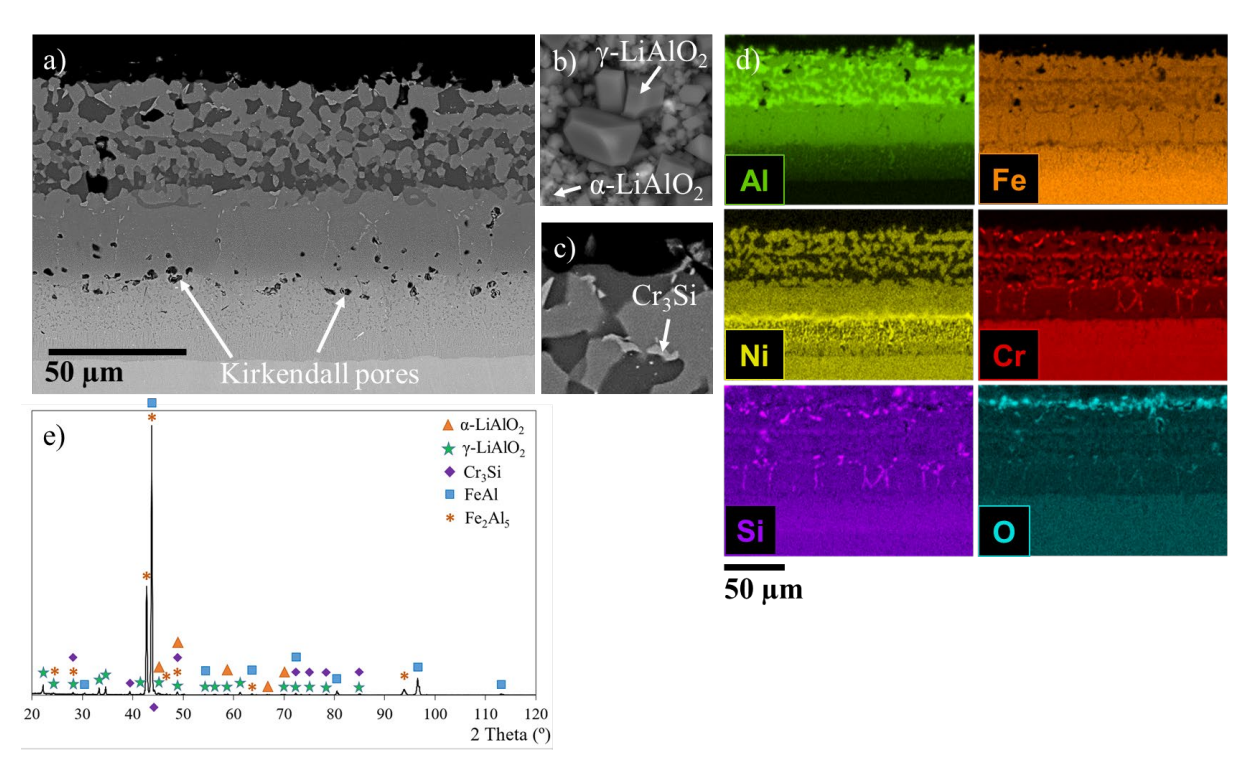


Figure 7. Analyses of the aluminide coated 347H after 500 h in ternary molten carbonate mixture at 700 °C: a), b) and c) FESEM micrographs of cross-section of the coating, focus on the mix α/γ LiAlO₂ layer formed on the coating surface exposed to the melt, and focus on Cr-Si precipitates formed in the coating top layer, respectively. Figure d) is an EDS elemental mapping of Al, Fe, Ni, Cr, Si and O from area in a). Figure e) is the corresponding surface XRD pattern.

4. Conclusion

Hot corrosion in Li-Na-K molten carbonates at 700 °C as well as cracking susceptibility of a newly developed aluminide coated 347H austenitic steel were investigated. A multi-layered coating was produced with an Al content reaching 69 at.% on top surface. Gravimetric results showed a significant improvement of the hot corrosion behavior of the coated alloy compared to the uncoated one. This was confirmed by cross-section observations: a multi-layered Li, Fe, Cr and Mn rich thick scale formed on the bare 347H, whereas slight changes were observed on the coated material after 500 h-exposure in the corrosive melt. In addition, the formation of a mix of α/γ -LiAlO₂ on the top surface evidenced a high corrosion protection which will be further confirmed after longer exposures. In parallel, the coating showed heterogeneous mechanical properties evidenced by the broad variation of hardness values and the formation of cracks at 4.5 % of deformation.

Data availability statement

Data availability can be sought by contacting Loïc Oger or Pauline Audigié at INTA.

Author contributions

Loïc Oger: Conceptualization, Methodology, Validation, Formal analysis, Data curation, Investigation, Writing – original draft, Writing – review & editing.

Alina Agüero: Writing – review & editing.

Pauline Audigié: Conceptualization, Methodology, Supervision, Project administration, Writing – review & editing.

Competing interests

The authors declare that they have no competing interests.

Funding

This project has received funding from the European Union in the framework of the HORIZON-MSCA-2022-PF-01 under the Grant Agreement of the Project: 101107201 — CoMeTES. Views and opinions expressed are however those of the author(s) only and do not necessarily reflect those of the European Union. Neither the European Union nor the granting authority can be held responsible for them.

Acknowledgement

The authors would like to thank the members of the Area of Metallic Materials at INTA for their invaluable technical assistance, EDF for providing the materials, the European Union's Horizon Europe research and innovation program that financed this project and Aurélien Prillieux for conducting the local hardness measurements and for the fruitful discussions.

References

- [1] "REPowerEU: Joint European Action for more affordable, secure and sustainable energy," *Eur. Comm.*, 2022.
- [2] MIT, The future of Energy Storage, vol. 1–3. 2023.
- [3] M. Medrano, A. Gil, I. Martorell, X. Potau, and L. F. Cabeza, "State of the art on high-temperature thermal energy storage for power generation. Part 2-Case studies," *Renew. Sustain. Energy Rev.*, vol. 14, no. 1, pp. 56–72, 2010, doi: 10.1016/j.rser.2009.07.036.
- [4] Concentrating solar power: Clean power on demand 24/7. The World Bank, 2020.
- [5] P. Audigié *et al.*, "High temperature molten salt corrosion behavior of aluminide and nickelaluminide coatings for heat storage in concentrated solar power plants," *Surf. Coatings Technol.*, vol. 349, no. May, pp. 1148–1157, 2018, doi: 10.1016/j.surfcoat.2018.05.081.
- [6] C. Prieto, S. Fereres, F. J. Ruiz-Cabañas, A. Rodriguez-Sanchez, and C. Montero, "Carbonate molten salt solar thermal pilot facility: Plant design, commissioning and operation up to 700 °C," *Renew. Energy*, vol. 151, pp. 528–541, 2020, doi: 10.1016/j.renene.2019.11.045.
- [7] M. Mehos *et al.*, "Concentrating Solar Power Gen3 Demonstration Roadmap," Golden, CO (United States), Jan. 2017. doi: 10.2172/1338899.

- [8] C. S. Turchi, J. Vidal, and M. Bauer, "Molten salt power towers operating at 600–650 °C: Salt selection and cost benefits," *Sol. Energy*, vol. 164, no. January, pp. 38–46, 2018, doi: 10.1016/j.solener.2018.01.063.
- [9] P. Audigié, V. Encinas-Sánchez, S. Rodríguez, F. J. Pérez, and A. Agüero, "High temperature corrosion beneath carbonate melts of aluminide coatings for CSP application," *Sol. Energy Mater. Sol. Cells*, vol. 210, no. March, 2020, doi: 10.1016/j.solmat.2020.110514.
- [10] "ASTM A335/A335M-21a Standard Specification for Seamless Ferritic Alloy-Steel Pipe for High-Temperature Service," *ASTM*, 2022.
- [11] C. G. Dariva and A. F. Galio, "Corrosion inhibitors: Principles, mechanisms and applications," in *Developments in Corrosion Protection*, 2014, pp. 1–161.
- [12] J. C. Gomez-Vidal, A. G. Fernandez, R. Tirawat, C. Turchi, and W. Huddleston, "Corrosion resistance of alumina-forming alloys against molten chlorides for energy production. I: Preoxidation treatment and isothermal corrosion tests," *Sol. Energy Mater. Sol. Cells*, vol. 166, no. February, pp. 222–233, 2017, doi: 10.1016/j.solmat.2017.02.019.
- [13] A. Soleimani Dorcheh, R. N. Durham, and M. C. Galetz, "Solar Energy Materials & Solar Cells Corrosion behavior of stainless and low-chromium steels and IN625 in molten nitrate salts at 600 ° C," *Sol. Energy Mater. Sol. Cells*, vol. 144, no. 3, pp. 109–116, 2016, doi: 10.1016/j.solmat.2015.08.011.
- [14] J. Luo *et al.*, "Corrosion behavior of SS316L in ternary Li2CO3–Na2CO3–K2CO3 eutectic mixture salt for concentrated solar power plants," *Sol. Energy Mater. Sol. Cells*, vol. 217, no. September, p. 110679, 2020, doi: 10.1016/j.solmat.2020.110679.
- [15] L. González-Fernández, M. Intxaurtieta Carcedo, O. Bondarchuk, and Y. Grosu, "Dynamic Corrosion of Carbonate Salt for 3rd Generation CSP Plants," *SolarPACES Conf. Proc.*, vol. 1, pp. 1–8, 2024, doi: 10.52825/solarpaces.v1i.614.
- [16] Á. G. Fernández and L. F. Cabeza, "Molten salt corrosion mechanisms of nitrate based thermal energy storage materials for concentrated solar power plants: A review," *Sol. Energy Mater. Sol. Cells*, vol. 194, no. February, pp. 160–165, 2019, doi: 10.1016/j.solmat.2019.02.012.
- [17] P. Audigié *et al.*, "Aluminide slurry coatings for protection of ferritic steel in molten nitrate corrosion for concentrated solar power technology," *AIP Conf. Proc.*, vol. 1850, 2017, doi: 10.1063/1.4984416.
- [18] A. Agüero, P. Audigié, S. Rodríguez, V. Encinas-Sánchez, M. T. De Miguel, and F. J. Pérez, "Protective coatings for high temperature molten salt heat storage systems in solar concentration power plants," AIP Conf. Proc., vol. 2033, 2018, doi: 10.1063/1.5067095.
- [19] M. Akita, Y. Uematsu, T. Kakiuchi, M. Nakajima, and Y. Nakamura, "Effect of Laves Phase Precipitation on Fatigue Properties of Niobium-containing Austenitic Stainless Steel Type 347 in Laboratory Air and in 3%NaCl Solution," *Procedia Mater. Sci.*, vol. 3, pp. 517–523, 2014, doi: 10.1016/j.mspro.2014.06.086.
- [20] "Norma Española UNE-EN ISO 6507-1," 2018.
- [21] A. Agüero, M. Gutiérrez, and V. González, "Deposition process of slurry iron aluminide coatings," *Mater. High Temp.*, vol. 25, no. 4, pp. 257–265, 2008, doi: 10.3184/096034008X388812.
- [22] P. Matysik, S. Józwiak, and T. Czujko, "Characterization of low-symmetry structures from phase equilibrium of Fe-Al system-microstructures and mechanical properties," *Materials* (*Basel*)., vol. 8, no. 3, pp. 914–931, 2015, doi: 10.3390/ma8030914.
- [23] J. D. Osorio *et al.*, "Failure Analysis for Molten Salt Thermal Energy Storage Tanks for In-Service CSP Plants," 2024. [Online]. Available: www.nrel.gov/publications.
- [24] S. H. White and U. M. Twardoch, "The solubility and electrochemistry of alkali metal oxides in the molten eutectic mixture of lithium carbonate-sodium carbonate-potassium carbonate," *J. Appl. Electrochem.*, vol. 19, no. 6, pp. 901–910, 1989, doi: 10.1007/BF01007939.
- [25] H. S. Hsu, J. H. DeVan, and M. Howell, "Solubilities of LiFeO2 and (Li, K)2CrO4 in Molten Alkali Carbonates at 650°C," *J. Electrochem. Soc.*, vol. 134, no. 9, pp. 2146–2150, 1987, doi: 10.1149/1.2100840.

- [26] P. Biedenkopf, M. Spiegel, and H. J. Grabke, "The corrosion behavior of Fe-Cr alloys containing Co, Mn, and/or Ni and of a Co-base alloy in the presence of molten (Li,K)-carbonate," *Mater. Corros. Werkstoffe und Korrosion*, vol. 48, no. 11, pp. 731–743, 1997, doi: 10.1002/maco.19970481103.
- [27] Y. Zhou *et al.*, "Precipitation behavior of type 347H heat-resistant austenitic steel during long-term higherature aging," *J. Mater. Res.*, vol. 30, no. 23, pp. 3642–3652, 2015, doi: 10.1557/jmr.2015.343.
- [28] J. Luo *et al.*, "Robust corrosion performance of cold sprayed aluminide coating in ternary molten carbonate salt for concentrated solar power plants," *Sol. Energy Mater. Sol. Cells*, vol. 237, no. December 2021, p. 111573, 2022, doi: 10.1016/j.solmat.2021.111573.
- [29] E. Hamdy, J. N. Olovsjö, and C. Geers, "Perspectives on selected alloys in contact with eutectic melts for thermal storage: Nitrates, carbonates and chlorides," *Sol. Energy*, vol. 224, no. October 2020, pp. 1210–1221, 2021, doi: 10.1016/j.solener.2021.06.069.